Volume 58
Number 64
18 August 2022
Pages 8873–9040

ChemComm

Chemical Communications

rsc.li/chemcomm

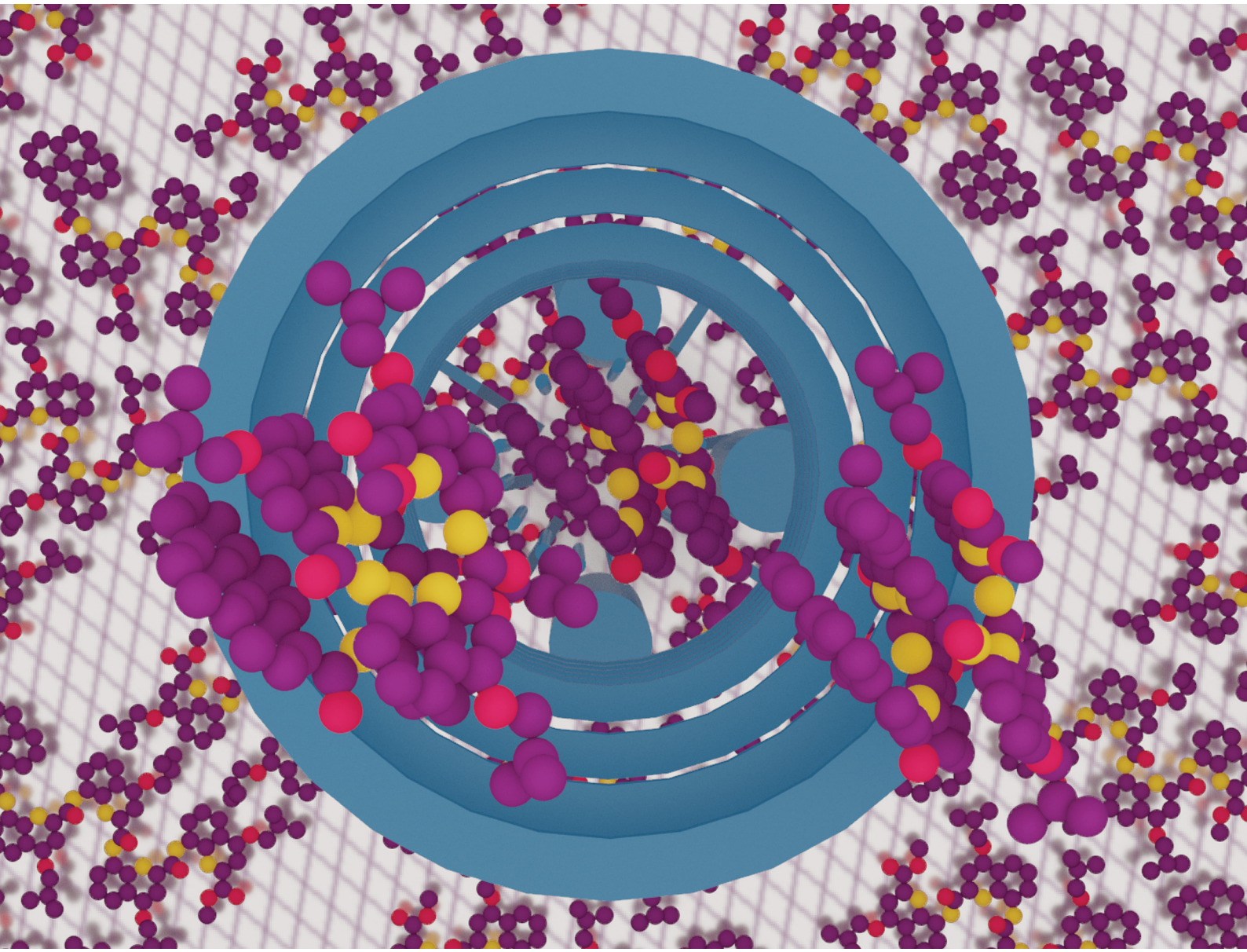

ISSN 1359-7345

ROYAL SOCIETY OF CHEMISTRY

COMMUNICATION

Anthoula C. Papageorgiou, Ivan Huc *et al.*
Structural adaptations of electrosprayed aromatic oligoamide foldamers on Ag(111)

ChemComm

COMMUNICATION

View Article Online
View Journal | View Issue

Cite this: *Chem. Commun.*, 2022, **58**, 8938

Received 10th June 2022,
Accepted 8th July 2022

DOI: 10.1039/d2cc03286d

rsc.li/chemcomm

Structural adaptations of electrosprayed aromatic oligoamide foldamers on Ag(111)†

Dennis Meier, ‡[a] Benedikt Schoof,‡[a] Jinhua Wang,[b] Xuesong Li,[b] Andreas Walz,[a] Annette Huettig,[a] Hartmut Schlichting,[a] Frédéric Rosu,[c] Valérie Gabelica,[cd] Victor Maurizot,[b] Joachim Reichert,[a] Anthoula C. Papageorgiou, *[a] Ivan Huc *[ef] and Johannes V. Barth[af]

Aromatic foldamers are promising for applications such as molecular recognition and molecular machinery. For many of these, defect free, 2D-crystaline monolayers are needed. To this end, submonolayers were prepared in ultra-high vacuum (UHV) on Ag(111) *via* electrospray controlled ion beam deposition (ES-CIBD). On the surface, the unfolded state is unambiguously identified by real-space single-molecule imaging using scanning tunnelling microscopy (STM) and it is found to assemble in regular structures.

Aromatic foldamers adopt particularly stable and predictable conformations and constitute useful molecular platforms for applications in molecular recognition,[1–6] transport through bilayer membranes[7–9] or molecular machinery.[10–12] They also feature interesting charge transport properties.[13–16] In the case of oligoamides of 8-amino-2-quinoline-carboxylic acid (Q_n, Fig. 1a), helical conformations are extremely stable in solution due to hydrogen bonding (dotted blue lines in Fig. 1a). An unfolding is also hindered through repulsive interaction between the oxygen atoms of the peptide bonds and the quinolines' nitrogen (grey arrows in Fig. 1a). For example, an octamer shows no denaturation at 120 °C in dimethyl sulfoxide[17] and its helix handedness inversion is kinetically locked in water.[18] These helices also feature strong resistance to mechanical extension.[19] No experimental conditions have been found to date under which unfolded (extended) or misfolded conformations would be significantly populated.

In the course of charge transport studies of these compounds, monolayers of thiol-functionalized helices on gold were produced.[14–16] Despite having the expected thickness for upstanding helices, these monolayers did not show high order, presumably due to limited surface diffusion preventing epitaxial growth. On the other hand, various helical polymers have been found to self-assemble on surfaces, albeit with their helix axes parallel to the surface plane.[20,21] We endeavoured into constructing 2D-crystalline monolayers of the previously described oligoamide foldamers by a completely different approach, using an in-house developed ES-CIBD system (Fig. 1e).[22,23] This method exploits electrospray ionisation to bring molecular ions to the gas phase and transfer them to UHV. After mass filtering, the extracted ions are soft landed on a solid surface with controlled energy and coverage.[24–26] ES-CIBD allows for the deposition of objects that would be too fragile, reactive or large for the sublimation required by organic molecular beam epitaxy.[27,28] Here we report of pyr-Q_4 and pyr-Q_7 oligomers revealing the formation of ordered arrays on an atomically planar Ag(111) surface in a surprising unfolded§ flat ribbon conformation (Fig. 1c and d) analysed by STM. Ag(111) is relatively inert and being dense packed and of low corrugation, it is a common substrate for the self-assembly of organic molecules. Complementary ion mobility measurements indicate that the ions are helically folded in the gas phase and the unfolding occurs on the metal surface.

Pyr-Q_4 and pyr-Q_7 (Fig. 1a, synthesis in ESI†) were designed with a pyrene foot expected to provide affinity to the surface yet without hampering mobility. As with the related aromatic foldamers, single crystal data show that pyr-Q_4 has a helical form (Fig. 1b, details in ESI†). Fig. 1f and g show the mass spectra for the two foldamer species measured with a digital quadrupole mass filter (dQMF) as part of the ES-CIBD system prior to deposition (see ESI† for experimental parameters). Pyr-Q_4 has only one peak at around 1230 Th, which corresponds to $[\text{pyr-}Q_4 + H]^+$ (see compound characterisation along with

[a] *Physics Department E20, Technical University Munich, D-85748 Garching, Germany. E-mail: a.c.papageorgiou@tum.de*
[b] *CBMN (UMR 5248), Univ. Bordeaux, CNRS, Bordeaux INP, F-33600 Pessac, France*
[c] *Institut Européen de Chimie et Biologie (UAR3033/US001), Univ. Bordeaux, CNRS, INSERM, F-33600 Pessac, France*
[d] *ARNA (U1212), Univ. Bordeaux, INSERM, CNRS, F-33600 Pessac, France*
[e] *Department of Pharmacy, Ludwig-Maximilians-University Munich, D-81377 Munich, Germany. E-mail: ivan.huc@cup.lmu.de*
[f] *Cluster of Excellence e-conversion, D-85748 Garching, Germany*

† Electronic supplementary information (ESI) available: Synthesis and analysis of new compounds, geometry optimisation of different rotamers on Ag(111), procedures of surface preparation, STM characterisation and ion mobility measurements. CCDC 2143687. For ESI and crystallographic data in CIF or other electronic format see DOI: https://doi.org/10.1039/d2cc03286d

‡ These authors contributed equally to this work.

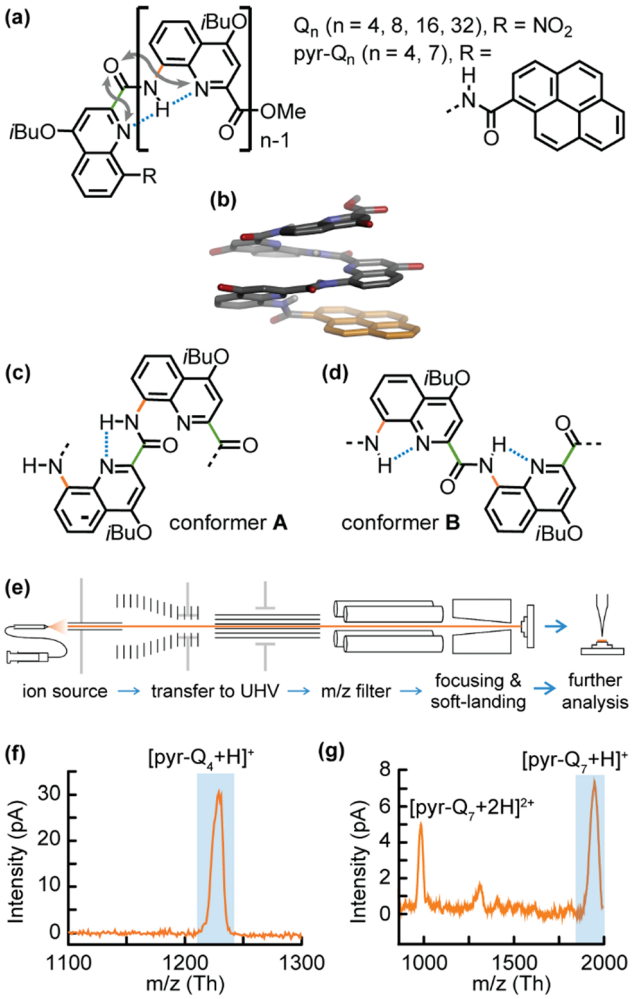

Fig. 1 (a) Structural formula of Q_n and pyr-Q_n foldamers. Blue dotted lines point out hydrogen bonds and grey arrows show electrostatic repulsion. The aryl–NH and aryl–carbonyl bonds are coloured in orange and green, respectively. (b) Crystal structure of pyr-Q_4 (isobutyl groups and hydrogen atoms omitted for clarity). Ribbon structures of unfolded§ molecule through either (c) rotation of the aryl-NH bonds (orange) or (d) rotation of the aryl–carbonyl bond (green). (e) Schematic of the ES-CIBD system. Mass spectra prior to ES-CIBD of (f) pyr-Q_4 and (g) pyr-Q_7. The *m*/*z* regions used for deposition are emphasized with blue badges.

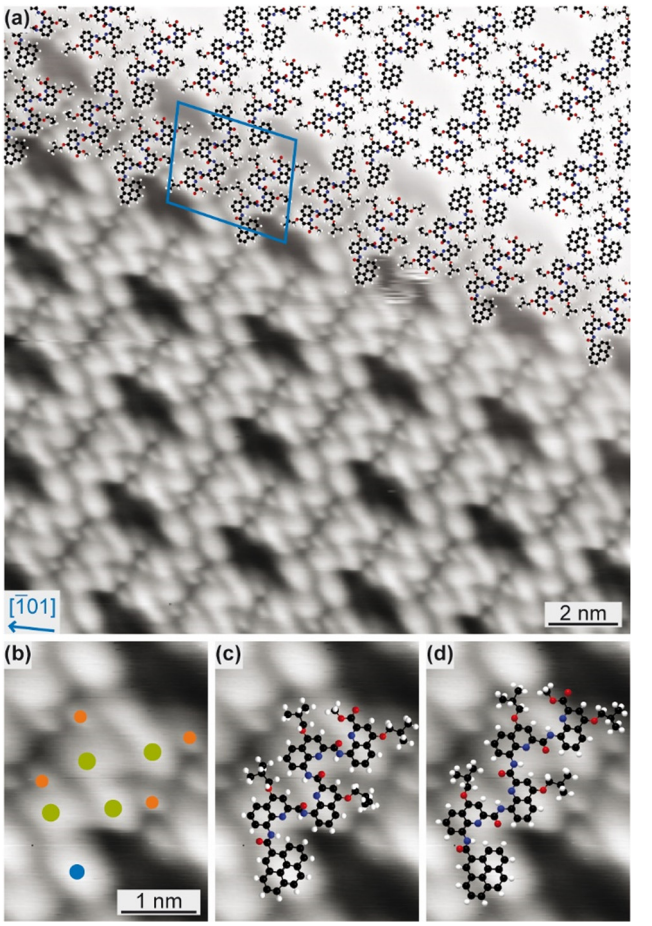

Fig. 2 STM of pyr-Q_4 on Ag(111). (a) Overview image (1500 mV, 100 pA, 170 K) partially overlaid with molecules. C, N, O and H atoms in black, blue, red and white, respectively. The unit cell is indicated in blue. A blue arrow shows a high symmetry direction of the Ag substrate. (b–d) High resolution STM image (1500 mV, 30 pA, 170 K). In (b) Blue, green and orange dots mark the moieties of a single molecule assigned to pyrene, quinoline and *i*BuO, respectively. Rotamer **A** and rotamer **B** are overlaid over the STM data in (c) and (d), respectively. Only rotamer **A** fits the STM data.

synthesis details in ESI†). Pyr-Q_7 has two major peaks at 1957 Th, $[\text{pyr-Q}_7 + \text{H}]^+$, and 979 Th, $[\text{pyr-Q}_7 + 2\text{H}]^{2+}$. Only the singly charged cations were deposited (blue windows in Fig. 1e and f). The additional protons of $[\text{pyr-Q}_n + \text{H}]^+$ species can transfer to the silver surface at room temperature (r.t.)[29,30] and form coadsorbed pyr-Q_n and atomic H. The latter species can recombine to form gaseous H_2.[31]

We started our investigation with the deposition of pyr-Q_4. The mean landing energy was set to $\sim$4.5 eV z^{-1} per molecule, as a trade-off of the ion current optimisation. The adsorbed pyr-Q_4 on Ag(111) was too mobile to image at r.t. Fig. 2a depicts the structure of a highly-ordered island stabilised at 170 K. Such islands extend over 60 nm (ESI,† Fig. S3b). Their arrangement is characterised by a unit cell containing two molecules rotated by 180° and can be described by the epitaxial matrix $\begin{pmatrix} 11 & 3 \\ 7 & 14 \end{pmatrix}$ (marked in blue in Fig. 2a). This corresponds to a density of 0.21 molecules per nm^2. A single molecule is identified by a constellation of five major protrusions (see blue and green dots in Fig. 2b) forming a zig-zag like structure and four small protrusions (orange dots in Fig. 2b) at the side. The latter can be associated with the iso-butoxy (*i*BuO) side groups at the quinoline core. Therefore, the protrusions marked green reflect the quinoline units. Notably, the terminal related protrusion is larger, presumably due to the methyl ester end group at the quinoline. The protrusion marked in blue can be assigned to the pyrene foot. Hence, the molecules appear adsorbed in an intact, unfolded§ yet organized, flat ribbon state on the Ag(111) surface. It is noted that the moieties capable of forming hydrogen bonds are distanced >4 Å between neighbouring molecules. Thus, intermolecular attractive van der Waals interactions between the *i*BuO side groups seem to play a significant

role in the self-assembly. Extended aromatic oligoamide ribbons were hitherto reported to form solely under a stretching force.[19] Nevertheless, less stable polyacetylene helices have also been shown to unfold into ribbons on graphite.[32] In fact, the conformational flexibility and unfolding of ribbons on surfaces may control their self-assembly, as exemplified recently by diene surface folding in open chains and shape-persistent macrocycles.[33]

To further understand the extended flat conformation of the adsorbed molecules, we considered different planar geometries. Rotations of the aryl-NH bonds (orange in Fig. 1c) and/or of the aryl–carbonyl bonds (green in Fig. 1d) between the quinolines can give rise to planar, ribbon conformations. Due to the regularity of the structure, we assumed that the same rotation takes place between every quinoline unit. With these considerations, two conformations of the extended foldamer were examined: through rotations of either all aryl–NH bonds (rotamer **A**) or all aryl–carbonyl bonds (rotamer **B**). The latter produces the most stretched conformation whereas the former corresponds to a shorter ribbon-like structure. The geometries of these rotamers on the Ag(111) surface were optimised by molecular mechanics (ESI,† Fig. S4a and b). Comparison with the high-resolution STM data (Fig. 2b and c) reveals that only rotamer **A** fits the STM image. This is somewhat surprising given the strong repulsion between iminic N and the carbonyl (Fig. 1c) in rotamer **A** which is in principle even less favoured than rotamer **B**: quantum mechanical calculations of model arylamide compounds report a 0.31 eV higher rotational barrier.[34] It is conceivable that this repulsion is partially compensated by the H^+ from the deposited species, as such protonation promotes unfolding in related oligomers.[35] Alternatively, electrostatic repulsions may be screened by the image charges in the metal surface.[36]

For comparison, the single positively charged $[\text{pyr-Q}_7 + H]^+$ was deposited by similar spraying parameters and landing energy per charge (4.5 eV z^{-1}). At 160 K, the molecules were found immobilised exclusively at the step edges of the Ag(111) surface (see Fig. 3a). Individual molecules are distinguished by eight major protrusions marked by green and blue dots in Fig. 3b. This corresponds well to the STM imaging of the extended pyr-Q_4 with five major protrusions (compare Fig. 2b and 3b). The protrusions assigned to the pyrene, quinoline, *i*BuO groups are marked by blue, green and orange dots, respectively (Fig. 3b). As for pyr-Q_4, the corresponding compact and extended rotamers **A′** and **B′** were considered and their geometries optimised on Ag(111) (ESI,† Fig. S4c and d). When the two simulated molecular structures are overlaid on the STM image (Fig. 3c and d), rotamer **B′** matches better (Fig. 3d) in contrast to rotamer **A** adopted by the smaller pyr-Q_4. It is therefore deduced that the unfolding occurs independently of the length of the foldamer and that different stereoisomers are expressed on the surface, presumably depending on the surface adsorption site (terrace *vs.* step edge). The presence of a folded pyr-Q_7 conformation on the Ag(111) surface cannot be excluded and might emerge by immobilising diffusing adsorbates at lower temperatures or of samples with higher molecular coverages. Further investigations of higher coverages are anticipated to reveal whether self-assembled pyr-Q_7 islands form, similar to pyr-Q_4.

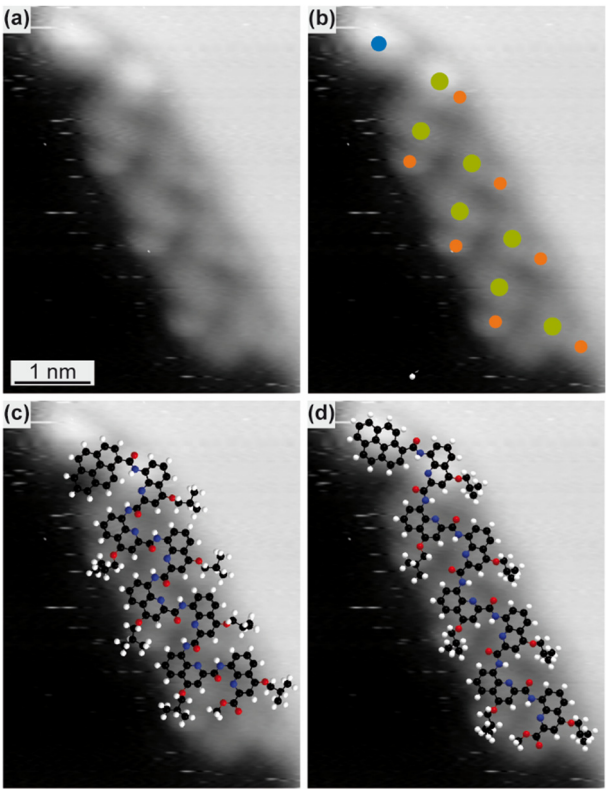

Fig. 3 (a) STM image (−1250 mV, −80 pA, 160 K) of pyr-Q_7 on a step edge of Ag(111) (b) pyrene, quinoline, *i*BuO groups marked on the STM image in blue, green and orange, respectively. STM image overlaid with (c) rotamer **A′** obtained through rotation of all aryl–NH bonds and (d) rotamer **B′** obtained through rotation of all the aryl–carbonyl bonds.

Following this analysis, the question arises whether the unfolding occurs during the spraying or upon adsorption. In solution, the helices of Q_n oligomers remain folded in acids as strong as pure trifluoroacetic acid. To investigate the potential destabilising effect of the ionising H^+ on the helix structure, ion mobility spectroscopy (IMS) measurements were carried out on a series of Q_n helical molecules with n ranging from 4 (less than two helix turns) to 32 (almost 13 helix turns). These experiments allow to estimate the size of ions in the gas phase after electrospray ionization. Fig. 4 shows a linear relation of the collisional cross section (CCS) of the different Q_n molecules and their mass. Calculated CCS values based on theoretically optimised structures are in excellent agreement with the experimental data (see ESI†). The linear evolution of the CCS with the size of the foldamer indicates a perfectly cylindrical (*i.e.* compact helical) shape and therefore a conservation of the foldamers' compact helical conformation in the gas phase. Notably, no changes of the CCS are found with increasing charge state up to four for Q_{32}. Thus, also Q_n molecules with higher charge state are in a helical structure during electrospray ionisation. Additionally, the charge states of pyr-Q_4 and pyr-Q_7 ions within

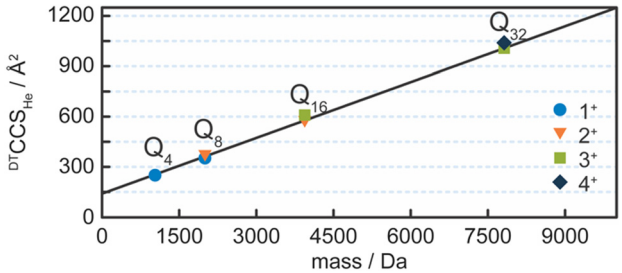

Fig. 4 Evolution of the collisional cross section ($^{DT}CCS_{He}$) as a function of the Q_n mass. The linear regression (R^2 = 0.99) indicates a perfectly cylindrical shape.

the presented experiments further support a helical structure (see ESI,† Section 4.1). It is thus reasonable to extrapolate that the pyr-Q_n molecules will retain their helical form following the electrospray ionisation and that the observed unfolding occurred on the Ag(111) surface.

A variety of factors can account for the structural change after landing. These include the high affinity of the aromatic units towards the metal surface, the screening of electrostatic repulsion by the metal surface (which eventually overrides intramolecular forces), deposition at r.t. and a kind of "reactive landing" caused by the impinging energy of 4.5 eV z^{-1}, which is considered to be "less soft".[25] This shall be evaluated in followup experiments.

In summary, we reported on the adsorption of flat extended pyr-Q_4 and pyr-Q_7 molecules on Ag(111) in UHV after deposition *via* ES-CIBD. As both pyr-Q_4 and pyr-Q_7 are mobile at r.t., the self-assembly scenario may be extended to other planar surfaces of inert metals, such as gold. Through IMS measurements, we determined that the electrospray ion beam contains helical molecules which unfold upon deposition on the metal surface. The insight provided by the present study is anticipated to be crucial in controlling the folding of biological and biomimetic molecules when integrated on surfaces.

This research was supported by the Deutsche Forschungsgemeinschaft (DFG) through the priority program COORNETs (SPP 1928), the Excellence Cluster e-conversion, and the Agence Nationale de la Recherche (ANR-18-CE29-0013-POLYnESI). We thank B. Kauffmann for assistance with X-ray structure elucidation.

Conflicts of interest

There are no conflicts to declare.

Notes and references

§ Unfolding often refers to a disordered conformation, as in proteins. In contrast, the unfolded flat ribbons observed here have a well-defined structure.

1 R. B. Prince, S. A. Barnes and J. S. Moore, *J. Am. Chem. Soc.*, 2000, **122**, 2758–2762.
2 S. Saha, B. Kauffmann, Y. Ferrand and I. Huc, *Angew. Chem., Int. Ed.*, 2018, **57**, 13542–13546.
3 S. B. Seo, S. Lee, H.-G. Jeon and K.-S. Jeong, *Angew. Chem., Int. Ed.*, 2020, **59**, 10441–10445.
4 F. C. Parks, Y. Liu, S. Debnath, S. R. Stutsman, K. Raghavachari and A. H. Flood, *J. Am. Chem. Soc.*, 2018, **140**, 17711–17723.
5 Y. Wang, J. Xiang and H. Jiang, *Chem. – Eur. J.*, 2011, **17**, 613–619.
6 M. Inouye, M. Waki and H. Abe, *J. Am. Chem. Soc.*, 2004, **126**, 2022–2027.
7 A. Roy, J. Shen, H. Joshi, W. Song, Y.-M. Tu, R. Chowdhury, R. Ye, N. Li, C. Ren, M. Kumar, A. Aksimentiev and H. Zeng, *Nat. Nanotechnol.*, 2021, **16**, 911–917.
8 S. Qi, C. Zhang, H. Yu, J. Zhang, T. Yan, Z. Lin, B. Yang and Z. Dong, *J. Am. Chem. Soc.*, 2021, **143**, 3284–3288.
9 Y. Shen, F. Fei, Y. Zhong, C. Fan, J. Sun, J. Hu, B. Gong, D. M. Czajkowsky and Z. Shao, *ACS Cent. Sci.*, 2021, **7**, 2092–2098.
10 M. Gauthier, V. Koehler, C. Clavel, B. Kauffmann, I. Huc, Y. Ferrand and F. Coutrot, *Angew. Chem., Int. Ed.*, 2021, **60**, 8380–8384.
11 X. Wang, Q. Gan, B. Wicher, Y. Ferrand and I. Huc, *Angew. Chem., Int. Ed.*, 2019, **58**, 4205–4209.
12 V. Koehler, A. Roy, I. Huc and Y. Ferrand, *Acc. Chem. Res.*, 2022, **55**, 1074–1085.
13 X. Li, N. Markandeya, G. Jonusauskas, N. D. McClenaghan, V. Maurizot, S. A. Denisov and I. Huc, *J. Am. Chem. Soc.*, 2016, **138**, 13568–13578.
14 A. Méndez-Ardoy, N. Markandeya, X. Li, Y.-T. Tsai, G. Pecastaings, T. Buffeteau, V. Maurizot, L. Muccioli, F. Castet, I. Huc and D. M. Bassani, *Chem. Sci.*, 2017, **8**, 7251–7257.
15 P. Mateus, A. Jacquet, A. Méndez-Ardoy, A. Boulloy, B. Kauffmann, G. Pecastaings, T. Buffeteau, Y. Ferrand, D. M. Bassani and I. Huc, *Chem. Sci.*, 2021, **12**, 3743–3750.
16 J. Wang, B. Wicher, A. Méndez-Ardoy, X. Li, G. Pecastaings, T. Buffeteau, D. M. Bassani, V. Maurizot and I. Huc, *Angew. Chem., Int. Ed.*, 2021, **60**, 18461–18466.
17 H. Jiang, J.-M. Léger and I. Huc, *J. Am. Chem. Soc.*, 2003, **125**, 3448–3449.
18 S. J. Dawson, Á. Mészáros, L. Pethő, C. Colombo, M. Csékei, A. Kotschy and I. Huc, *Eur. J. Org. Chem.*, 2014, 4265–4275.
19 F. Devaux, X. Li, D. Sluysmans, V. Maurizot, E. Bakalis, F. Zerbetto, I. Huc and A.-S. Duwez, *Chem*, 2021, **7**, 1333–1346.
20 J. Kumaki, S.-I. Sakurai and E. Yashima, *Chem. Soc. Rev.*, 2009, **38**, 737–746.
21 J. Zhu, Z. Dong, S. Lei, L. Cao, B. Yang, W. Li, Y. Zhang, J. Liu and J. Shen,, *Angew. Chem., Int. Ed.*, 2015, **54**, 3097–3101.
22 A. Walz, K. Stoiber, A. Huettig, H. Schlichting and J. V. Barth, *Anal. Chem.*, 2022, **94**, 7767–7778.
23 W. Ran, A. Walz, K. Stoiber, P. Knecht, H. Xu, A. C. Papageorgiou, A. Huettig, D. Cortizo-Lacalle, J. P. Mora-Fuentes, A. Mateo-Alonso, H. Schlichting, J. Reichert and J. V. Barth, *Angew. Chem., Int. Ed.*, 2022, **61**, e202111816.
24 G. Verbeck, W. Hoffmann and B. Walton, *Analyst*, 2012, **137**, 4393–4407.
25 K. Anggara, Y. Zhu, M. Delbianco, S. Rauschenbach, S. Abb, P. H. Seeberger and K. Kern, *J. Am. Chem. Soc.*, 2020, **142**, 21420–21427.
26 J. Laskin, G. E. Johnson, J. Warneke and V. Prabhakaran, *Angew. Chem., Int. Ed.*, 2018, **57**, 16270–16284.
27 W.-P. Peng, M. P. Goodwin, Z. Nie, M. Volný, Z. Ouyang and R. G. Cooks, *Anal. Chem.*, 2008, **80**, 6640–6649.
28 S. Rauschenbach, F. L. Stadler, E. Lunedei, N. Malinowski, S. Koltsov, G. Costantini and K. Kern, *Small*, 2006, **2**, 540–547.
29 M. Röckert, M. Franke, Q. Tariq, D. Lungerich, N. Jux, M. Stark, A. Kaftan, S. Ditze, H. Marbach, M. Laurin, J. Libuda, H.-P. Steinrück and O. Lytken, *J. Phys. Chem. C*, 2014, **118**, 26729–26736.
30 S. Massicot, T. Sasaki, M. Lexow, S. Shin, F. Maier, S. Kuwabata and H.-P. Steinrück, *Langmuir*, 2021, **37**, 11552–11560.
31 G. Lee, P. T. Sprunger, M. Okada, D. B. Poker, D. M. Zehner and E. W. Plummer, *J. Vac. Sci. Technol., A*, 1994, **12**, 2119–2123.
32 S.-i Sakurai, K. Okoshi, J. Kumaki and E. Yashima, *Angew. Chem., Int. Ed.*, 2006, **45**, 1245–1248.
33 S. Kim, H. D. Castillo, M. Lee, R. D. Mortensen, S. L. Tait and D. Lee, *J. Am. Chem. Soc.*, 2018, **140**, 4726–4735.
34 A. M. Abramyan, Z. Liu and V. Pophristic, *Chem. Commun.*, 2016, **52**, 669–672.
35 C. Dolain, V. Maurizot and I. Huc, *Angew. Chem., Int. Ed.*, 2003, **42**, 2738–2740.
36 A. Schiffrin, J. Reichert, Y. Pennec, W. Auwärter, A. Weber-Bargioni, M. Marschall, M. Dell'Angela, D. Cvetko, G. Bavdek, A. Cossaro, A. Morgante and J. V. Barth, *J. Phys. Chem. C*, 2009, **113**, 12101–12108.